A Three-Dimensional Extended Sb Network in the Metallic Antimonides $(M',Ti)_5Sb_8$ (M' = Zr, Hf, Nb, Mo)

Holger Kleinke[†]

Department of Chemistry, University of Waterloo, Waterloo, Ontario, Canada N2L 3G1

Received July 12, 2000

$(M',Ti)_5Sb_8$ was prepared from the melt by arc-melting suitable mixtures of Ti, $TiSb_2$, and $M'Sb_2$, respectively. This phase exists at least with M' = Zr, Hf, Nb, and Mo. A significant phase range for $Zr_\delta Ti_{5-\delta}Sb_8$ was found to be within $1.10(8) \le \delta \le 3.9(3)$. All $(M',Ti)_5Sb_8$ representatives investigated occur in the same, yet hitherto unknown structure type, as determined by single-crystal analyses. E.g., the lattice dimensions of $Zr_\delta Ti_{5-\delta}Sb_8$ range from a = 654.49(3) pm, c = 2662.4(2) pm for δ = 1.10(8) to a = 671.06(6), c = 2679.7(4) pm for δ = 3.9(3) (space group $I4_122$, No. 98, Z = 4). The three chemically inequivalent metal sites are statistically occupied by different mixtures of the M atoms M' and Ti, included in a three-dimensional network of Sb atoms on 6- to 8-fold Sb coordinated positions. Sb−Sb bonds of intermediate lengths occur in addition to the predominating heteronuclear M−Sb bonds. Physical property measurements of $(Zr,Ti)_5Sb_8$ reveal these phases being metallic exhibiting specific resistances of several mΩ·cm and a small Seebeck coefficient at room temperature, in agreement with the results of the electronic structure calculations on the LMTO and extended Hückel levels. The calculations indicate a possible change to semiconducting properties by heavy doping.

Introduction

Among the Sb-rich transition metal antimonides, the filled skutterudites LnM_4Sb_{12} (Ln = lanthanoid, M = Fe, Co, Ni, ...)[1] have attracted wide interest based on their enhanced thermoelectric properties which result mainly from the low thermal conductivity.[2] The rattling of the Ln atom, which is located in a cage of Sb atoms, leads to an effective scattering of the phonons, thus causing the extraordinarily low thermal conductivity.[3] The use of the skutterudites as thermoelectric materials at elevated temperatures, however, is inhibited by their decomposition points of ca. 1000 K.

In an attempt to improve on the latter while conserving the other physical properties, one might want to turn to the Sb-rich antimonides of the valence-electron-poor, for simplicity often called "early", transition elements because of their higher melting/decomposition points which are related to the higher covalency of the metal−Sb bonds. However, no promising binary candidate was found in the literature, as all of the antimonides MSb_2 (M = Ti, Zr, Hf, V, Nb, Ta) known in this class are reported or calculated to be metallic.[4,5] Note that metallic properties most likely lead to unfavorable thermoelectric properties, since the Seebeck coefficients are expected to be very low. Most reasonably good thermoelectric materials exhibit small band gaps, i.e., are so-called good semiconductors, and rather complicated densities of states in the vicinity of the Fermi level.[6−8] Other criteria for enhanced thermoelectric properties are small differences in the electronegativities of the constituent elements, heavy constituent elements, crystal structures exhibiting low symmetry, mixed occupancies on several sites in the structures, and eventually rattling of atoms, which would be expressed in high displacement parameters.[9] Most recently, Kanatzidis et al. discovered a new thermoelectric material, namely, $CsBi_4Te_6$, which is most promising for low-temperature applications.[10]

We thought of different approaches to achieve nonmetallic properties of the early transition metal antimonides. We are currently investigating several pseudobinary systems $(M,M')_xSb$, searching for new compounds with small band gaps. The fact that mixing two related metal atoms may lead to the formation of new antimonides was successfully demonstrated with the discoveries of $(Hf,Ti)_7Sb_4$,[11] $(Zr,V)_{11}Sb_8$,[12] $(Zr,V)_{13}Sb_{10}$,[13] and (Zr,Ti)Sb,[14] using the DFSO concept (differential fractional site occupancies on the metal positions) introduced by Franzen et al.[15,16]

With this article, we present the first results, which comprise new Sb-rich phases consisting of titanium and a second early transition metal M' (M' = Zr, Hf, Nb, Mo). These phases occur in a new structure type and exhibit a metal:antimony ratio of 5:8, which is unprecedented among the transition metal antimonides. The crystal structure, the electronic structure, and the physical properties including the Seebeck coefficient (sometimes

[†] Fax: +1 (519) 746-0435. E-mail: kleinke@uwaterloo.ca.

(1) Jeitschko, W.; Braun, D. *Acta Crystallogr.* **1977**, *B33*, 7.
(2) Sales, B. C.; Mandrus, D.; Williams, R. K. *Science* **1996**, *272*, 1325.
(3) Morelli, D. T.; Meisner, G. P. *J. Appl. Phys.* **1995**, *77*, 3777.
(4) Villars, P. *Pearson's Handbook, Desk Edition*; American Society for Metals: Materials Park, OH, 1997.
(5) Kleinke, H. Unpublished calculations.
(6) Rowe, D. M. *CRC Handbook of Thermoelectrics*; CRC Press: Boca Raton, FL, 1995.
(7) Kanatzidis, M. G.; McCarthy, T. J.; Tanzer, T. A.; Chen, L.-H.; Iordanis, L. *Chem. Mater.* **1996**, *8*, 1465.
(8) Chung, D.-Y.; Jobic, S.; Hogan, T.; Kannewurf, C. R.; Brec, R.; Rouxel, J.; Kanatzidis, M. G. *J. Am. Chem. Soc.* **1997**, *119*, 2505.
(9) DiSalvo, F. J. *Science* **1999**, *285*, 703.
(10) Chung, D.-Y.; Hogan, T.; Brazis, P.; Rocci-Lane, M.; Kannewurf, C.; Bastea, M.; Uher, C.; Kanatzidis, M. G. *Science* **2000**, *287*, 1024.
(11) Kleinke, H. *Inorg. Chem.* **1999**, *38*, 2931.
(12) Kleinke, H. *J. Mater. Chem.* **1999**, *9*, 2703.
(13) Kleinke, H. *Chem. Commun. (Cambridge)* **1998**, 2219.
(14) Kleinke, H. *J. Am. Chem. Soc.* **2000**, *122*, 853.
(15) Yao, X.; Marking, G. A.; Franzen, H. F. *Ber. Bunsen-Ges. Phys. Chem.* **1992**, *96*, 1552.
(16) Franzen, H. F.; Köckerling, M. *Prog. Solid State Chem.* **1995**, *23*, 265.

10.1021/ic000767s CCC: $20.00
Published on Web 12/07/2000

Table 1. Crystallographic Data for $(M',Ti)_5Sb_8$

chemical formula	$Zr_{1.10(8)}Ti_{3.90}Sb_8$	$Zr_{2.6(3)}Ti_{2.4}Sb_8$	$Zr_{3.9(3)}Ti_{1.1}Sb_8$	$Hf_{2.6(1)}Ti_{2.4}Sb_8$
fw/(g/mol)	1261.2	1327.2	1381.4	1549.8
T/K	295	295	295	295
space group	$I4_122$ (No. 98)	$I4_122$ (No. 98)	$I4_122$ (No. 98)	$I4_122$ (No. 98)
a/pm	654.49(3)	665.06(6)	671.06(6)	661.37(7)
c/pm	2662.4(2)	2668.0(4)	2679.7(4)	2685.0(5)
V/(10^6 pm^3)	1140.5(1)	1180.1(2)	1206.7(2)	1174.4(3)
Z	4	4	4	4
calcd density/(g·cm^{-3})	7.35	7.47	7.60	8.77
abs coeff/cm^{-1}	220.7	216.5	214.2	422.0
$R(F_o)$,[a] $R_w(F_o^2)$[b]	0.030, 0.066	0.048, 0.108	0.046, 0.106	0.029, 0.037

[a] $R(F_o) = \sum||F_o| - |F_c||/\sum|F_o|$. [b] $R_w(F_o^2) = [\sum[w(F_o^2 - F_c^2)^2]/\sum[w(F_o^2)^2]]^{1/2}$.

Table 2. Positional Parameters and Equivalent Displacement Parameters

					U_{eq}/pm^2			
atom	site	x[a]	y[a]	z[a]	$Zr_{1.1}Ti_{3.9}Sb_8$	$Zr_{2.6}Ti_{2.4}Sb_8$	$Zr_{3.9}Ti_{1.1}Sb_8$	$Hf_{2.6}Ti_{2.4}Sb_8$
Sb1	8e	0.8281(2)	$\bar{x}$	0	124(3)	177(7)	139(7)	109(9)
Sb2	16g	0.2035(3)	0.3418(2)	0.06153(4)	160(2)	205(5)	209(6)	144(6)
Sb3	8f	0.6564(3)	1/4	1/8	233(5)	299(10)	309(11)	221(12)
M1	8c	0	0	0.0977(2)	103(7)	119(11)	108(10)	73(7)
M2	8c	1/2	0	0.0468(2)	128(9)	150(20)	110(20)	126(14)
M3	4b	1/2	1/2	0	165(13)	280(40)	290(30)	170(20)

[a] Values for $Zr_{1.1}Ti_{3.9}Sb_8$.

misleadingly called thermopower) are discussed, as are the relations to binary antimonides, especially to $TiSb_2$[17] and $ZrSb_2$.[18]

Experimental Section

Synthesis. The binary antimonides $TiSb_2$, $ZrSb_2$, $HfSb_2$,[19] and $NbSb_2$[20] were prepared first for use as starting materials. For these syntheses, the elements were mixed in the stoichiometric 1:2 ratio and then placed into a silica tube, which was subsequently sealed under vacuum. The mixtures were heated in conventional tube furnaces over a period of 3−7 days at 650 °C, i.e., slightly above the melting point of antimony (630 °C). Guinier diagrams taken after the reactions indicate the presence of the desired antimonides MSb_2 in quantitative yields.

The main reaction was carried out by arc-melting cold-pressed pellets under a flow of argon of 3 L/min, the pellets consisting of the previously prepared antimonides MSb_2 and additional metal in powder form, following the scheme in eq 1. The excess of antimony was used to compensate for evaporation losses. EDX analyses of the vapor showed the presence of antimony only and proved the metal:antimony ratio to be 5:8. No impurities were detected.

$1 < \delta \leq 4$:

$$(4.5 - \delta)TiSb_2 + \delta M'Sb_2 + 0.5Ti \rightarrow M'_\delta Ti_{5-\delta}Sb_8 + Sb\uparrow \quad (1)$$

Single phase samples could be obtained for $Zr_\delta Ti_{5-\delta}Sb_8$ with δ being within $1 < \delta < 4$; reactions aiming at $\delta < 1$ or $\delta > 4$ resulted in the formation of $TiSb_2$ or $ZrSb_2$ as the main products. First substitution attempts also yielded isostructural $(Hf,Ti)_5Sb_8$ (nominal Hf:Ti ratio = 1:1), $(Nb,Ti)_5Sb_8$ (Nb:Ti = 1:4, with $Nb_\delta Ti_{1-\delta}Sb_2$ as a major side product), and $(Mo,Ti)_5Sb_8$ (Mo:Ti = 1:4). For the latter, the reaction was started from Mo, Ti, and $TiSb_2$, since the only known binary molybdenum antimonide, Mo_3Sb_7, decomposes above 780 °C into the elements.[21] $(Mo,Ti)_5Sb_8$ was observed only in poor yields, besides unreacted $TiSb_2$ and elemental Mo.

Table 3. Occupancy Factors f_{Ti} of the Metal Sites[a]

M site	$Zr_{1.10(8)}Ti_{3.90}Sb_8$	$Zr_{2.6(3)}Ti_{2.4}Sb_8$	$Zr_{3.9(3)}Ti_{1.1}Sb_8$	$Hf_{2.6(1)}Ti_{2.4}Sb_8$
M1	0.72(2)	0.36(4)	0.07(4)	0.41(1)
M2	0.73(2)	0.48(7)	0.37(6)	0.46(3)
M3	1.00	0.69(9)	0.25(8)	0.66(3)

[a] Assuming full occupancy, i.e., $1 = f_{Ti} + f_{M'}$.

The shifts of the lines in the powder patterns reveal a decrease in the lattice dimensions by going from Zr_4TiSb_8 through $ZrTi_4Sb_8$ through $(Nb,Ti)_5Sb_8$ to $(Mo,Ti)_5Sb_8$, which reflects the different atomic radii ($r_{Ti} < r_{Zr}$; $r_{Zr} > r_{Nb} > r_{Mo}$). In addition to the powder diagrams, the products were confirmed via EDX analyses using an electron microscope with an additional EDX device. Attempts to prepare a M_5Sb_8 phase without Ti or with only Ti as the M atom failed so far.

Structure Determination. For the investigations of the phase range of $Zr_\delta Ti_{5-\delta}Sb_8$, we collected single-crystal data sets on selected single crystals with nominal Zr:Ti ratios of 1:4, 1:1, and 4:1. The structure solutions and refinements using SHELXS/SHELXL[22] were straightforward, except that mixed Zr/Ti occupancies had to be assumed. The refinement procedures were carried out as described recently for (Zr,Ti)-Sb. To prove that the same structure occurs in the other systems with Hf, Nb, and Mo, we tried to find suitable single crystals containing these elements as well. However, we succeeded only in the case with Hf as the third constituent element besides Ti and Sb, while a Nb-containing crystal gave reasonable lattice dimensions (a = 650.19(8) pm, c = 2638.1(4) pm, $V = 1115.2(3) \times 10^6$ pm^3, nominal Nb:Ti ratio = 1:4), but diffracted too poorly for a refineable data set. Crystallographic details may be found in Table 1. Positional parameters, equivalent displacement parameters, and occupancy factors are listed in Tables 2 and 3, respectively.

Band Structure Calculations. For the calculations, we chose the structure of $Zr_{1.1}Ti_{3.9}Sb_8$ as experimentally determined, all M sites treated as being occupied solely by Ti, i.e., modeling hypothetical *Ti_5Sb_8*, since mixed occupancies cannot be handled within the theories. The extended Hückel theory[23−25] was used to calculate the Mulliken overlap populations for the different interactions, which serve as a

(17) Havinga, E. E.; Damsma, H.; Hokkeling, P. *J. Less-Common Met.* **1972**, *27*, 169.
(18) Kjekshus, A. *Acta Chem. Scand.* **1972**, *26*, 1633.
(19) Schubert, K.; Frank, K.; Gohle, R.; Maldonado, A.; Meissner, H. G.; Raman, A.; Rossteutscher, W. *Naturwissenschaften* **1963**, *50*, 41.
(20) Furuseth, S.; Kjekshus, A. *Nature* **1964**, *203*, 512.
(21) Brown, A. *Nature* **1965**, *206*, 502.
(22) Sheldrick, G. M. *SHELXS-86/SHELXL-97*; University of Göttingen: Göttingen, Germany, 1986−1997.
(23) Hoffmann, R. *J. Chem. Phys.* **1963**, *39*, 1397.
(24) Whangbo, M.-H.; Hoffmann, R. *J. Am. Chem. Soc.* **1978**, *100*, 6093.
(25) Program EHMACC, adapted for use on a PC by M. Köckerling, Gesamthochschule Duisburg, 1997.

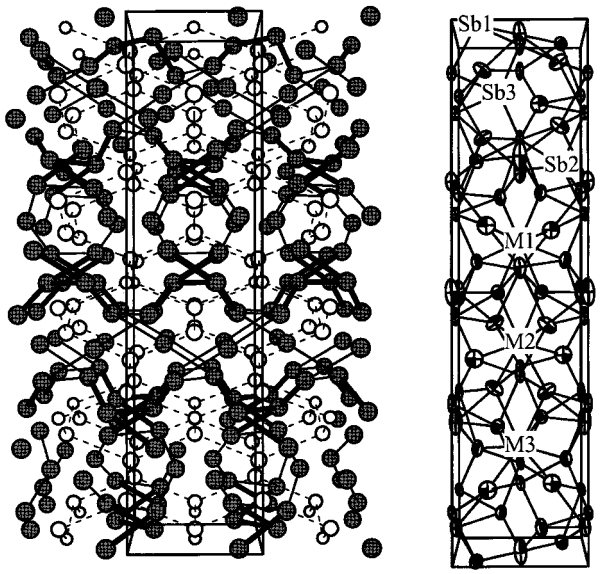

Figure 1. Projection of the structure of $Zr_{2.6}Ti_{2.4}Sb_8$ along [100]. Vertical: *c* axis. Left: large, gray circles, Sb; small, white circles, M atoms. Higher Zr contents are reflected in larger circles. Thick lines: Sb−Sb bonds < 320 pm. Thin lines: 330 pm < d_{Sb-Sb} < 345 pm. Dashed lines: d_{M-M} < 370 pm. M−Sb bonds are omitted for the sake of clarity. Right: unit cell showing anisotropic displacement parameters, atom labels, and M−Sb bonds only.

Table 4. Parameters Used for Extended Hückel Calculations on the Model Structure Ti_5Sb_8

orbital	H_{ii}/eV	ς_1	c_1	ς_2	c_2
Ti, 4s	−7.775	1.50			
Ti, 4p	−4.050	1.50			
Ti, 3d	−8.033	4.55	0.4391	1.600	0.7397
Sb, 5s	−18.80	2.32			
Sb, 5p	−11.70	2.00			

relative measure for bond strengths,[26] using a mesh of 112 *k* points of the first Brillouin zone of the primitive unit cell. After taking the Hückel parameters for Ti and Sb from standard sources,[27] the ionization potential parameters of Ti were optimized by charge iteration on $TiSb_2$ (Table 4).

Since the Hückel theory depends strongly on the parameters used, self-consistent tight-binding LMTO calculations (LMTO = linear muffin tin orbitals)[28−30] were carried out in order to get more reliable results for the band structure. Therein, the density functional theory is used with the local density approximation (LDA). The integration in *k* space was performed by an improved tetrahedron method[31] on a grid of 1030 irreducible *k* points of the first Brillouin zone (DOS and COHP:[32] 234 *k* points). Principal differences in the results of Hückel and LMTO calculations were discussed before and occur here also.[33,34]

Physical Property Measurements. The properties of a sample of the nominal composition $Zr_1Ti_4Sb_8$ were determined. Temperature dependent resistance measurements down to 10 K were performed on a cold-pressed bar of the dimensions 0.2 cm × 0.1 cm × 0.25 cm applying a four-contact method. Absolute Seebeck coefficients were determined on the same cold-pressed bar at room temperature applying six different temperature gradients in order to check for consistency.

(26) Mulliken, R. S. *J. Chem. Phys.* **1955**, *23*, 2343.
(27) Clementi, E.; Roetti, C. *At. Data Nucl. Data Tables* **1974**, *14*, 177.
(28) van Barth, U.; Hedin, L. *J. Phys.* **1971**, *C4*, 2064.
(29) Andersen, O. K. *Phys. Rev.* **1975**, *B12*, 3060.
(30) Skriver, H. L. *The LMTO Method*; Springer: Berlin, 1984.
(31) Blöchl, P. E.; Jepsen, O.; Andersen, O. K. *Phys. Rev.* **1994**, *B49*, 16223.
(32) Dronskowski, R.; Blöchl, P. *J. Phys. Chem.* **1993**, *97*, 8617.
(33) Kleinke, H.; Felser, C. *J. Solid State Chem.* **1999**, *144*, 330.
(34) Kleinke, H.; Felser, C. *J. Alloys Compd.* **1999**, *291*, 73.

Table 5. Selected Interatomic Interactions

		d/pm[a]	d/pm[b]	d/pm[c]	d/pm[d]	MOP[e]	PBO[e]
Sb1−Sb1	1×	318.2(2)	317.5(4)	318.5(4)	317.0(5)	0.157	0.214
−Sb2	2×	315.5(2)	318.0(4)	319.4(4)	317.1(6)	0.216	0.237
Sb2−Sb1	1×	315.5(2)	318.0(4)	319.4(4)	317.0(5)	0.216	0.237
−Sb3	1×	329.1(1)	333.4(3)	336.1(3)	333.5(8)	0.143	0.141
−Sb2	1×	337.4(2)	340.7(5)	341.6(5)	340.4(7)	0.068	0.102
Sb3−Sb2	2×	329.1(1)	333.4(3)	336.1(3)	333.6(5)	0.143	0.141
M1−Sb2	2×	277.6(2)	283.1(5)	285.9(4)	281.1(5)	0.411	0.776
−Sb3	2×	287.4(2)	292.4(4)	294.8(4)	291.0(5)	0.340	0.533
−Sb2	2×	294.7(5)	296.3(9)	296.8(7)	296.9(7)	0.294	0.403
−Sb1	2×	304.9(5)	306.1(9)	308.3(7)	307.9(7)	0.182	0.272
−M2	2×	354.2(3)	359.9(6)	364.0(4)	359.6(4)	0.047	0.031
−M1	2×	358.1(3)	362.2(6)	364.4(4)	360.4(5)	0.046	0.027
M2−Sb1	2×	272.6(3)	276.6(5)	278.3(4)	274.6(5)	0.462	0.940
−Sb3	2×	283.9(4)	286.5(8)	289.7(6)	288.3(6)	0.447	0.610
−Sb2	2×	298.7(2)	304.6(4)	308.5(4)	302.3(5)	0.258	0.345
−Sb2	2×	334.1(5)	333.7(1)	333.2(7)	333.5(8)	0.065	0.089
−M3	2×	350.2(2)	354.9(4)	357.3(3)	352.7(3)	0.044	0.037
−M1	2×	354.2(3)	359.9(6)	364.0(4)	359.6(4)	0.046	0.031
M3−Sb2	4×	274.3(1)	276.4(3)	278.9(3)	276.6(4)	0.509	0.881
−Sb1	2×	303.7(1)	311.5(3)	315.3(3)	309.1(4)	0.220	0.285
−M2	4×	350.2(2)	354.9(4)	357.3(3)	352.7(3)	0.044	0.037

[a] $Zr_{1.1}Ti_{3.9}Sb_8$. [b] $Zr_{2.6}Ti_{2.4}Sb_8$. [c] $Zr_{3.9}Ti_{1.1}Sb_8$. [d] $Hf_{2.6}Ti_{2.4}Sb_8$. [e] *Ti_5Sb_8*; MOP, Mulliken overlap population; PBO, Pauling bond order.

Results and Discussion

Crystal Structure. The crystal structure of $(M',Ti)_5Sb_8$ is depicted in Figure 1, showing $Zr_{2.6}Ti_{2.4}Sb_8$ as one representative. This presentation was chosen to give an impression of the complexity of the crystal structure, emphasizing the three-dimensional extended network of Sb atoms. The heteronuclear M−Sb interactions, which dominate by far with respect to number and shortness, are omitted in the left part of Figure 1 for clarity.

For the major interactions are the M−Sb bonds, they are discussed first on the basis of the local coordination spheres. Every M atom is surrounded by six (M3) to eight (M1 and M2) Sb atoms in the first coordination spheres. The closest M atoms appear in the second coordination sphere; every M atom is surrounded by four other M atoms in distances between 350 and 360 pm (Table 5). Remarkable are the significant differences in the Sb surroundings of the M atoms. In $ZrTi_4Sb_8$, the M1 atom is coordinated by eight Sb atoms in distances between 278 and 305 pm which form a quite irregular polyhedron. M2 is surrounded by six Sb atoms (d = 273−299 pm) and two farther apart ones (d = 334 pm), corresponding to a (6 + 2)-coordination. On the other hand, M3 is coordinated by four Sb2 (distance d = 274 pm) and two Sb1 atoms (d = 304 pm), which can be viewed as a (4 + 2)-coordination. All of these distances except the largest one (334 pm) increase in the series $Zr_\delta Ti_{5-\delta}Sb_8$ with increasing Zr content, reflecting the differences in the Pauling single bond radii (r_{Ti} = 132, r_{Zr} = 145 pm)[35] as well as in Slater's empirical atomic radii (r_{Ti} = 140, r_{Zr} = 155 pm).[36] Typical Ti−Sb distances include 280 pm in TiSb (coordination number CN = 6)[37] and 292 pm in $TiSb_2$ (CN = 8), and typical Zr−Sb distances range from 284 to 311 pm in ZrSb (CN = 5−7)[38] and from 295 to 303 pm in $ZrSb_2$ (CN = 8−9). Correspondingly, the Zr content per M site increases with increasing CN and increasing M−Sb distances in the three studied examples of $(Zr,Ti)_5Sb_8$, as was also observed in the representatives of the (Zr,Ti)Sb phase. The analogous trends

(35) Pauling, L. *The Nature of the Chemical Bond*, 3rd ed.; Cornell University Press: Ithaca, NY, 1948.
(36) Slater, J. C. *J. Chem. Phys.* **1964**, *41*, 3199.
(37) Nowotny, H.; Peal, J. *Monatsh. Chem.* **1951**, *82*, 336.
(38) Garcia, E.; Corbett, J. D. *J. Solid State Chem.* **1988**, *73*, 452.

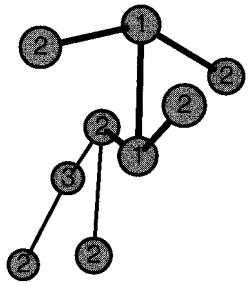

Figure 2. Part of the Sb network showing the strongest Sb−Sb bonds, emphasizing the $(Sb2-Sb1-Sb2)_2$ unit via thick lines.

take place in $(Hf,Ti)_5Sb_8$, also, since the size of a Hf atom is comparable to that of a Zr atom (e.g., Pauling radius $r_{Hf} = 144$ pm, Slater $r_{Hf} = 155$ pm).

On the other hand, the (pseudo)homonuclear distances, i.e., M−M and Sb−Sb, are rather long, which is especially true for the M−M distances. With more than 350 pm in length, these contacts are longer than in the corresponding binary antimonides, e.g., $d_{Ti-Ti} = 315$ pm in TiSb and 290 pm in $TiSb_2$, and $d_{Zr-Zr} = 339-340$ pm in ZrSb and 344 pm in $ZrSb_2$. Especially in the case of the Ti-rich $(M',Ti)_5Sb_8$ phases, the M−M interactions are assumed to be at best very weak. This is reflected in small Pauling bond orders, which are calculated according to the equation $d(n) = d(1) - 60$ pm $\times \log n$ (with n = bond order). Using $d(1) = 2r_{Ti} = 264$ pm, the largest M−M Pauling bond orders (PBOs) are 0.04 in $ZrTi_4Sb_8$ (as listed in Table 5), compared to 0.14 in TiSb and 0.37 in $TiSb_2$.

The Sb−Sb distances, however, are intermediate in length, starting at 316 pm (PBO = 0.22). This is significantly longer than typical single bonds, as found in the structures of KSb (283 and 285 pm),[39] *cyclo*-Sb_5^{5-} (between 281 and 291 pm),[40] and Sb_{11}^{3-} (between 276 and 285 pm),[41] or the shortest bond in elemental antimony (291 pm). Single Sb−Sb bonds are also present in $TiSb_2$ (284 pm) and $ZrSb_2$ (288 pm), and bonds comparable to those in M_5Sb_8 occur in ZrSb (324−325 pm). The Sb−Sb bond of 326 pm in Li_2Sb has a bond order of $^1/_2$,[42] which is comparable to the Sb−Sb distances in M_5Sb_8. The shortest Sb−Sb distances in M_5Sb_8 are much shorter than the interlayer distance of 335 pm in elemental antimony, the three-dimensional mechanical properties of which suggest at least modest, but definitely positive, orbital overlap between the Sb atoms of neighboring layers.

Concentrating on the shortest Sb−Sb bonds in M_5Sb_8, the Sb atom substructure comprises oligomer Sb_6 units, interconnected via longer Sb−Sb contacts (329−342 pm, depicted in Figure 2 by thin lines) to the three-dimensional extended Sb atom network. The Sb_6 unit comprises two nonlinear Sb_3 chains (Sb2−Sb1−Sb2), which are arranged in a staggered conformation and connected through a bond between the central Sb1 atoms.

Electronic Structure. Considering the M−M interactions in a first approximation as negligible, one can assign formal oxidation states of +4 for the M atoms and—on average—of −2.5 for the Sb atoms, i.e., every Sb atom needs $^1/_2$ electron to gain a filled octet. On the basis of the electronegativities of the metal atoms and antimony (e.g., Allred and Rochow electronegativities, Ti 1.32, Zr 1.22, Sb 1.82, or Pauling, Ti 1.54, Zr 1.33, Sb 2.05), this assignment of oxidation states is as valid as oxidation states of +1 for H and −4 for C in CH_4 with electronegativities of 2.20 for H and 2.50−2.55 for C.

Following this argumentation, every Sb atom may form one Sb−Sb bond with a bond order of $^1/_2$, or a correspondingly higher number of fractional bonds. Summing over all Sb−Sb bonds <340 pm per Sb atom yields total Sb−Sb Pauling bond orders (PBOs) of 0.69 for Sb1, 0.48 for Sb2, and 0.28 for Sb3, which averages to PBO = 0.48 ≈ $^1/_2$ per Sb atom in $ZrTi_4Sb_8$. This correlates well with the formulation $(M^{+4})_5(Sb^{-2.5})_8$ despite the lack in precision of the PBO method.

More reliable results were obtained using the extended Hückel approximation to calculate the Mulliken overlap populations (MOPs). The MOPs calculated for hypothetical *Ti_5Sb_8* reveal bonding character of all interactions <350 pm. The multitude of M−Sb bonds all have MOPs between +0.51 and +0.14 electron per bond, which are most definitely positive and thus indicative of strong bonding character. Similarly, the MOPs of the Sb−Sb distances <350 pm vary from +0.22 (316 pm) to +0.07 (337 pm), suggesting that all of these are significantly bonding as well, as comparable values show: typical Sb−Sb bonds exhibit MOPs of 0.65 (for the single bonds in KSb), 0.62 (single bond in $TiSb_2$), 0.53 (291 pm) and 0.08 (335 pm) in elemental antimony. Note that the latter, the interlayer interaction, is proven to be bonding because of the three-dimensional physical and mechanical properties of antimony. Interactions with a bond order of $^1/_2$ exhibit MOPs of roughly 0.3 electron per bond, e.g., 0.26 in La_3TiSb_5,[43] 0.38 in (Zr,Ti)Sb, 0.34 in $(Zr,V)_{11}Sb_8$, and 0.36 in $(Zr,V)_{13}Sb_{10}$. The smaller MOPs correspond to those found for Sb−Sb distances between 324 and 350 pm, e.g., in ZrSb (0.06−0.09), $Zr_3Ni_3Sb_4$ (0.03),[44] and (Zr,Ti)Sb (0.03−0.07), indicating weak bonding interactions in every case. Even longer contacts were discovered to be of bonding nature, e.g., in $[(CH_3)_2Sb-Sb(CH_3)_2]_2$ by measurements of the force constant (0.125 N·cm^{-1}) of the intermolecular Sb−Sb interaction (368 pm), which is about 11% of the value for the intramolecular single bond of 284 pm (1.1 N·cm^{-1}).[45] For a detailed overview, see ref 46.

The cumulated Sb−Sb MOPs per Sb atom follow the same trend as the PBOs, i.e., MOP(Sb1) = 0.59 > MOP(Sb2) = 0.43 > MOP(Sb3) = 0.28. The fact that stronger Sb−Sb interactions occur with a smaller reduction of the Sb atoms and therefore smaller Mulliken gross populations was shown earlier in the reports dealing with $Zr_2V_6Sb_9$,[47] $(Hf,Ti)_7Sb_4$, (Zr,Ti)Sb, $(Zr,V)_{11}Sb_8$, and $(Zr,V)_{13}Sb_{10}$ and is also reflected in the electronic structure of *Ti_5Sb_8*: the Mulliken populations increase from Sb1 (5.12) over Sb2 (5.27) to Sb3 (5.40).

Last, the Mulliken overlap populations of the M−M distances suggest weak, but apparently bonding character: the MOPs range from +0.04 to +0.05, thus being smaller than in TiSb (d = 315 pm, MOP = 0.16), $TiSb_2$ (d = 290 pm, MOP = 0.18), and elemental titanium (d = 289 pm, MOP = 0.24; d = 295 pm, MOP = 0.22). It is concluded that the structures of the M_5Sb_8 phases are stabilized to some extent by (pseudo)-homonuclear M−M and Sb−Sb interactions, in addition to the predominating M−Sb bonds. Therefore, some d electrons must remain centered at the M atoms, i.e., they are not completely oxidized, and the oxidation states must thus be smaller than +4.

(39) Hönle, W.; von Schnering, H.-G. *Z. Kristallogr.* **1981**, *155*, 307.
(40) Korber, N.; Richter, F. *Angew. Chem., Int. Ed. Engl.* **1997**, *36*, 1512.
(41) Bolle, U.; Tremel, W. *J. Chem. Soc., Chem. Commun.* **1992**, 91.
(42) Müller, W. *Z. Naturforsch.* **1977**, *B32*, 357. Papoian, G. A.; Hoffmann, R. *Angew. Chem., Int. Ed.* **2000**, *39*, 2408.
(43) Bolloré, G.; Ferguson, M. J.; Hushagen, R. W.; Mar, A. *Chem. Mater.* **1995**, *7*, 2229.
(44) Wang, M.; McDonald, R.; Mar, A. *Inorg. Chem.* **1999**, *38*, 3435.
(45) Bürger, H.; Eujen, R.; Becker, G.; Mundt, O.; Westerhausen, M.; Witthauer, C. *J. Mol. Struct.* **1983**, *98*, 265.
(46) Kleinke, H. *Chem. Soc. Rev.* **2000**, *29*, 411.
(47) Kleinke, H. *Eur. J. Inorg. Chem.* **1998**, 1369.

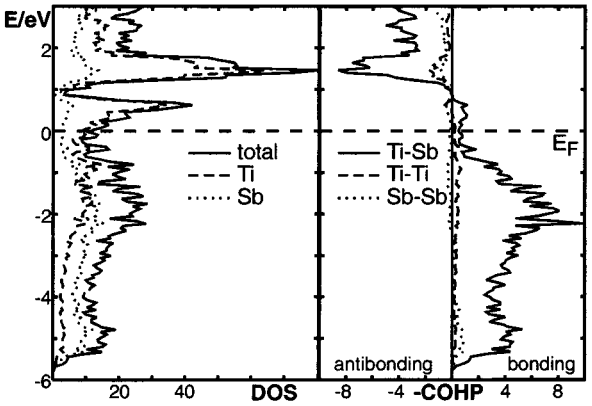

Figure 3. DOS (left) and COHP curves (right) of the model structure Ti_5Sb_8.

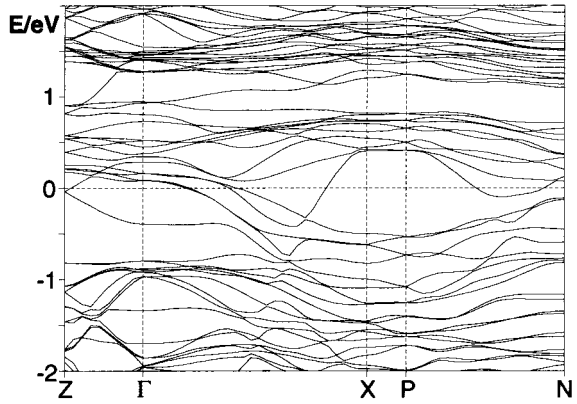

Figure 4. Band structure of the model structure Ti_5Sb_8.

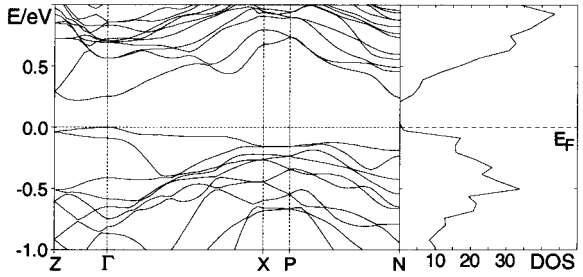

Figure 5. Band structure (left) and DOS (right) of the model structure Mo_5Sb_8 in the vicinity of the Fermi level.

These considerations are also supported by the results of the LMTO calculations. The densities of states (DOS) and their projections on the Ti and Sb atoms, respectively, are shown in the left part of Figure 3. Two main peaks occur within the energy window shown, the first (at the bottom between −6 and 0 eV) comprises Sb p states (dotted line), and the second (starting around −1 eV) mainly consists of Ti d states (dashed line). Both peaks overlap strongly, and the Fermi level E_F (held at 0.0 eV) is located above the lower part of the Ti peak, with a significant number of states filled directly at E_F, while a tail of the Sb peak goes well above E_F. Thus, the Sb atoms are rather far—though not completely—reduced, whereas some Ti electrons remain available for the formation of Ti−Ti bonds. Furthermore, the contributions of the Ti atoms at lower energies (i.e., below ca. −1 eV) to the Sb-dominated region result from strong mixing and therefore suggest covalent character of the Ti−Sb interactions.

The crystal orbital Hamiltonian populations (COHP curves), as obtained by weighing up the densities of states, are exhibited in the right part of Figure 3 cumulated over all bonds per primitive unit cell for the three different kinds of interactions in Ti_5Sb_8, namely, Ti−Sb (solid line), Ti−Ti (dashed), and Sb−Sb (dotted). The dominance of the heteronuclear Ti−Sb interactions is obvious. Only bonding Ti−Sb and Ti−Ti states are filled, whereas antibonding Sb−Sb states start to become filled at ca. −2.5 eV below E_F. However, clearly more bonding than antibonding Sb−Sb states are filled, confirming the overall bonding character of the Sb−Sb interactions. It should be noted that the huge differences between the M−Sb and Sb−Sb bonds are in part a consequence of the different multitude.

A gap is found in the COHP curves, about 0.8 eV above E_F, which separates bonding Ti−Sb from antibonding Ti−Sb interactions. The gap in the COHPs is reflected in a pseudo band gap in the DOS curve. Raising the Fermi level by increasing the number of valence electrons to this gap (i.e., 10 electrons per formula unit) would result in a gain in M−Sb and M−M interactions, but a (minor) loss in Sb−Sb interaction due to more filled antibonding states.

While the densities of states, being a projection of the band structure, already suggest metallic character of Ti_5Sb_8, the band structure itself has to be exploited to see if bands actually do cross the Fermi level. We therefore show the dispersion of the bands along four selected symmetry lines, with the special k points chosen according to Bradley and Cracknell.[48] According to the calculation, Ti_5Sb_8 exhibits three-dimensional metallic properties, as some bands directly cut E_F along Γ−Z (parallel to c^*) and Γ−X (parallel to a^*).

The band structure also reveals that a band gap might easily open up at ca. +0.8 eV above E_F. To check whether this could happen, we calculated the band structure for hypothetical Mo_5Sb_8 in the $(M',Ti)_5Sb_8$ structure, using different decreased unit cell parameters between a = 630 and 650 pm and c = 2500 and 2630 pm, since Mo atoms are smaller than Ti (after Pauling: r_{Mo} = 122 pm). Within this range of lattice parameters, the results all were the same: hypothetical Mo_5Sb_8 exhibits a small band gap (ca. 0.3 eV) directly at the Fermi level (Figure 5). It can thus be concluded that a M_5Sb_8 phase with 70 valence electrons—provided it can be synthesized—is semiconducting.

We already found the M_5Sb_8 structure in the Nb−Ti−Sb and Mo−Ti−Sb systems, which proves that the number of valence electrons can be modified to some extent. However, the preparation of a M_5Sb_8 phase with 70 valence electrons has yet to be done, which could possibly be achieved by substituting on the Sb sites as well. E.g., the hypothetical antimonide telluride $Mo_{5-\delta}Ti_\delta Sb_{8-2\delta}Te_{2\delta}$ would possess 70 valence electrons per formula unit.

Physical Properties. The metallic character of $(M',Ti)_5Sb_8$ with 60 valence electrons, e.g., M′ = Zr or Hf, as proposed on the basis of the band structure of hypothetical Ti_5Sb_8, is supported by the results obtained experimentally. For example, the specific resistance of Zr_4TiSb_8 is 16 mΩ·cm at room temperature, decreasing slowly without anomalies with decreasing temperature (Figure 6). While the slope is typical for metals, the absolute value of the specific resistance is approximately 10^4 higher than the one of elemental copper, the commercially mostly used metallic conductor. Although this difference is probably partly due to grain boundaries, we characterize $(Zr,Ti)_5Sb_8$ as a poorly conducting metal. In addition, Zr_4TiSb_8 exhibits a Seebeck coefficient of −0.5(1) μV/K at ambient conditions, which compares well with other n-type metals, i.e., niobium (−0.44 μV/K) or rhenium (−5.9 μV/K).

(48) Bradley, C. J.; Cracknell, A. P. *The Mathematical Theory of Symmetry in Solids*; Clarendon Press: Oxford, 1972.

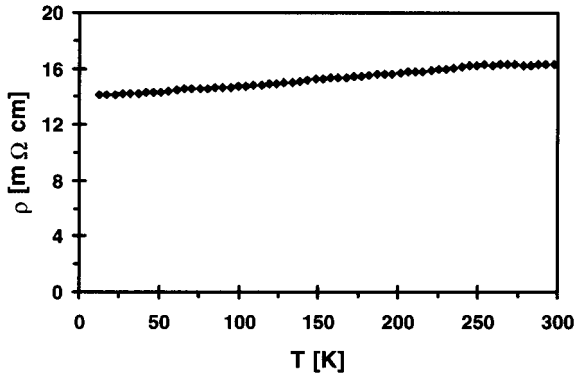

Figure 6. Temperature dependence of the specific resistance of Zr_4TiSb_8.

Conclusion

The new phases $M'_\delta Ti_{5-\delta}Sb_8$ exist at least with M′ = Zr, Hf, Nb, and Mo, and $1.10(8) \leq \delta \leq 3.9(3)$ in the case of M′ = Zr. The hitherto unknown $(M',Ti)_5Sb_8$ structure comprises a three-dimensional extended Sb atom substructure, which includes three chemically inequivalent metal sites M1−3, being statistically occupied by different mixtures of M′ and Ti. The structure is stabilized by the dominating M−Sb bonds as well as homonuclear Sb−Sb and also—to the smallest extent—by (pseudo)homonuclear M−M bonds. With 60 valence electrons, i.e., M′ = Zr and Hf, $(M',Ti)_5Sb_8$ is metallic, as shown by resistance and Seebeck coefficient measurements. On the other hand, a hypothetical M_5Sb_8 phase with 70 valence electrons, e.g., $Mo_{5-\delta}Ti_\delta Sb_{8-2\delta}Te_{2\delta}$, should be semiconducting with a band gap of ca. 0.3 eV, according to the LMTO calculations. Such a compound—provided it would form—should be an ideal candidate for use in thermoelectric energy conversion. Aside from the charge carrier concentration, the antimonides M_5Sb_8 comply with the other basic criteria for enhanced thermoelectrics, namely, a crystal structure exhibiting low symmetry compared to the skutterudites or Bi_2Te_3, mixed occupancies on the three M sites, and partly enlarged atomic displacement parameters. Therefore, the synthesis of a M_5Sb_8 phase with 70 valence electrons remains as a challenging goal.

Acknowledgment. This work was initiated at the Department of Chemistry of the University of Marburg in Germany, supported by the BMFT, DFG, and FCI. Ongoing funding from MMO and NSERC is appreciated.

Supporting Information Available: Four X-ray crystallographic files, in CIF format. This material is available free of charge via the Internet at http://pubs.acs.org.

IC000767S